BIOCHEMISTRY
including biophysical chemistry & molecular biology

Article

pubs.acs.org/biochemistry

Characterization of a Cobalt-Specific P_{1B}-ATPase

Eliza L. Zielazinski,[†] George E. Cutsail III,[†] Brian M. Hoffman,[†] Timothy L. Stemmler,*[,‡] and Amy C. Rosenzweig*[,†]

[†]Departments of Molecular Biosciences and Chemistry, Northwestern University, Evanston, Illinois 60208, United States

[‡]Department of Biochemistry and Molecular Biology and Cardiovascular Research Institute, Wayne State University, School of Medicine, Detroit, Michigan 48201, United States

Supporting Information

ABSTRACT: The P_{1B}-type ATPases are a ubiquitous family of P-type ATPases involved in the transport of transition metal ions. Divided into subclasses based on sequence characteristics and substrate specificity, these integral membrane transporters play key roles in metal homeostasis, metal tolerance, and the biosynthesis of metalloproteins. The P_{1B-4}-ATPases have the simplest architecture of the five P_{1B}-ATPase families and have been suggested to play a role in Co^{2+} transport. A P_{1B-4}-ATPase from *Sulfitobacter* sp. NAS-14.1, designated sCoaT, has been cloned, expressed, and purified. Activity assays indicate that sCoaT is specific for Co^{2+}. A single Co^{2+} binding site is present, and optical, electron paramagnetic resonance, and X-ray absorption spectroscopic data are consistent with tetrahedral coordination by oxygen and nitrogen ligands, including a histidine and likely a water. Surprisingly, there is no evidence for coordination by sulfur. Mutation of a conserved cysteine residue, Cys 327, in the signature transmembrane Ser-Pro-Cys metal binding motif does not abolish the ATP hydrolysis activity or affect the spectroscopic analysis, establishing that this residue is not involved in the initial Co^{2+} binding by sCoaT. In contrast, replacements of conserved transmembrane residues Ser 325, His 657, Glu 658, and Thr 661 with alanine abolish ATP hydrolysis activity and Co^{2+} binding, indicating that these residues are necessary for Co^{2+} transport. These data represent the first in vitro characterization of a P_{1B-4}-ATPase and its Co^{2+} binding site.

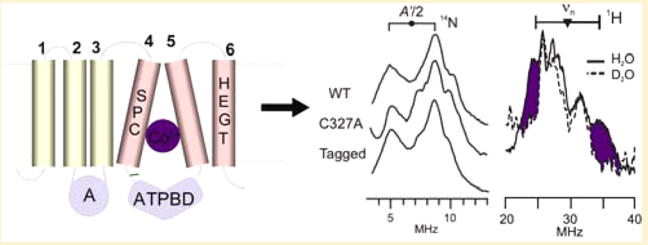

The P-type ATPases, found in a variety of species from bacteria to humans, are a family of integral transmembrane proteins that transport charged substrates across cell membranes using the energy provided by ATP hydrolysis.[1,2] P-type ATPases are divided into subclasses based on substrate specificity. These subclasses include the P_{1A}-ATPases (K^+), the P_{1B}-ATPases (heavy metals), the P_2-ATPases (Ca^{2+}, Na^+/K^+, and H^+/K^+), the P_3-ATPases (H^+), the P_4-ATPases (phospholipids), and the P_5-ATPases (unknown substrate).[3−5] All P-type ATPases share a common architecture consisting of multiple transmembrane (TM) helices, soluble nucleotide binding and phosphorylation domains (N- and P-domains, collectively termed the ATP binding domain or ATPBD), and a soluble actuator domain (A-domain). All P-type ATPases are believed to follow a Post−Albers mechanism in which catalytic phosphorylation of a conserved aspartic acid residue within an invariant DKTGT sequence in the P-domain causes conformational switching between an E1 high-affinity cation binding state and an E2 lower-affinity state[6−9] (Figure 1). Crystal structures are available for multiple conformational states of the sarcoplasmic reticulum Ca^{2+}-ATPase (SERCA),[10] and some structures of the Na^+/K^+-ATPase,[11,12] the H^+-ATPase,[13] and the Cu^+-ATPase[14] have also been determined.

The P_{1B}-type ATPases transport transition metal ions, including $Zn^{2+}/Cd^{2+}/Pb^{2+}$,[15−17] Cu^{2+},[18] Cu^+/Ag^+,[19,20] and Co^{2+}.[21] Members of the P_{1B} subgroup are widely distributed across all domains of life, conferring heavy metal tolerance and playing an essential role in the distribution of metal micronutrients and the biosynthesis of metalloproteins.[20,22] In humans, mutations in the Cu^+-ATPases ATP7A and ATP7B lead to Menkes syndrome and Wilson disease, respectively.[23] The core architectural features of the P_{1B}-type ATPases include at least six TM helices and two large cytoplasmic loops housing the ATPBD (containing the N- and P-domains) and the A-domain (Figure 2). The C-terminal TM helices 4−6 contain residues that are proposed to form the metal binding site(s), and the identities and positions of these residues are believed to determine metal specificity.[24] Mutagenesis data indicate that a three-residue cysteine-containing "signature" sequence motif in TM4 (CPC, CPH, SPC, and PCP) is of particular importance for metal transport activity.[25−29] On the basis of these signature sequence motifs and some experimental data, the P_{1B}-ATPases have been grouped into five substrate-specific subfamilies designated P_{1B-1} through P_{1B-5}.[24,30] The P_{1B-1}, P_{1B-2}, and P_{1B-3} subfamilies contain two additional TM helices at the N-terminus. The subfamilies are further differentiated according to the presence or absence of N- and/or C-terminal soluble

Received: May 22, 2012
Revised: September 11, 2012
Published: September 12, 2012

dx.doi.org/10.1021/bi3006708 | *Biochemistry* 2012, 51, 7891−7900

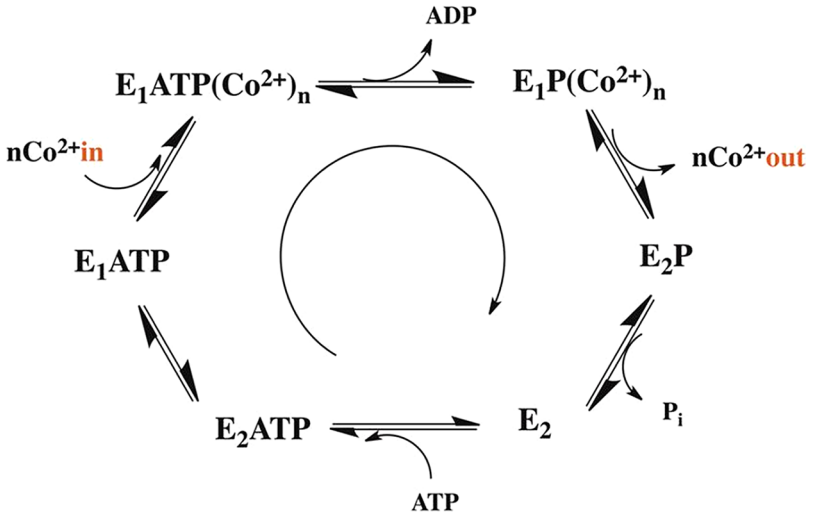

Figure 1. Post−Albers catalytic cycle represented for a Co^{2+}-ATPase. The cycle is defined by two conformational states (E1 and E2) that are interconverted by the covalent attachment and release of phosphate to and from a conserved aspartic acid residue. In the E1 state, which has high affinity for the substrate being transported, the binding site is accessible to the cytoplasm. Upon hydrolysis of ATP, a conformational change in the TM helices converts the binding site to being accessible to the periplasm (or other cellular compartment) and lowers the substrate affinity of E2. After the substrate is released, dephosphorylation occurs and the protein reverts to the E1 state.

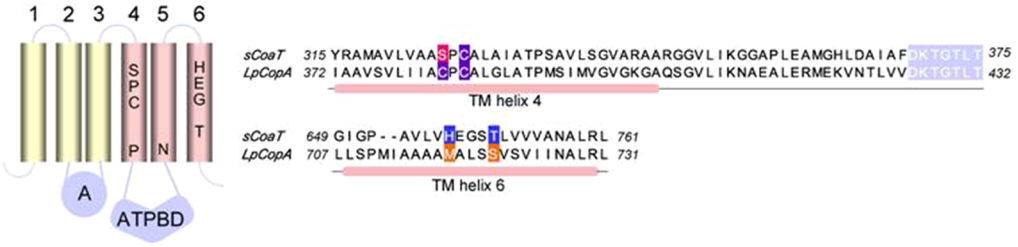

Figure 2. Architecture and key residues of P_{1B-4}-ATPases. Overall topology with conserved residues in TM helices shown in approximate locations (left). Noncontinuous alignment of TM helices 4 and 6 of sCoaT and LpCopA (right). The phosphorylation site in the P-domain is highlighted in light purple. Site I proposed metal-binding residues of LpCopA are colored orange, with the corresponding proposed sCoaT metal-binding residues colored blue. Site II residues of LpCopA are colored purple along with conserved sCoaT residues, and a nonconserved sCoaT residue is colored red.

metal-binding domains (MBDs), which likely regulate the ATPase function.[31−34]

The P_{1B-1}-ATPases are specific for Cu^+/Ag^+; the P_{1B-2}-ATPases are $Zn^{2+}/Cd^{2+}/Pb^{2+}$ transporters, and the P_{1B-3}-ATPases are specific for Cu^{2+}. Representative members of these three families have been purified and characterized biochemically.[17−19,25,35,36] In addition, a crystal structure of the *Legionella pneumophila* CopA P_{1B-1}-ATPase (LpCopA) has been determined recently.[14] Less is known about the P_{1B-4}- and P_{1B-5}-ATPases. While the P_{1B-4}-ATPases have been suggested to play a role in Co^{2+} transport,[21] their substrate specificity has not been established. The substrate for the P_{1B-5}-ATPases is unknown.[37] The P_{1B-4}-ATPases have the simplest architecture, with only six TM helices and no N- or C-terminal MBDs. A conserved Ser-Pro-Cys (SPC) motif is located in TM4 (Figure 2). Genetic data obtained more than 10 years ago for the *Synechocystis* PCC6803 P_{1B-4}-ATPase CoaT indicate that it is linked to Co^{2+} tolerance.[21] In *Cupriavidus metallidurans* CH34, the P_{1B-4}-ATPase CzcP is proposed to play a role in resistance to Zn^{2+}, Cd^{2+}, and Co^{2+}.[38] The plant P_{1B-4}-ATPase HMA1 transports Ca^{2+}, and expression of HMA1 in yeast confers tolerance to Zn^{2+}, Cd^{2+}, Co^{2+}, and Cu^+.[39,40] Thus, the metal substrate of the P_{1B-4}-ATPases has not yet been clearly defined, and no biochemical characterization of a purified P_{1B-4}-ATPase has been reported. To further understand this subfamily of P_{1B}-ATPases, we have expressed, purified, and characterized a P_{1B-4}-ATPase from *Sulfitobacter* sp. NAS-14.1, designated sCoaT. Isolated sCoaT binds Co^{2+} and exhibits Co^{2+}-induced ATPase activity. The Co^{2+} binding site has been probed by spectroscopy, and the roles of conserved residues have been assessed by mutagenesis. These data provide new insight into the function and properties of the P_{1B-4}-ATPase subfamily.

MATERIALS AND METHODS

Homology Modeling of sCoaT Based on LpCopA. Homology modeling of sCoaT and LpCopA was performed using DeepView (http://www.expasy.org/spdbv/).[41] Chain B of the LpCopA structure (PDB entry 3RFU) was used as the reference sequence onto which the sequence of sCoaT was mapped. Structural alignment was performed on the last four TM helices of both sCoaT and LpCopA (starting from TM helix 3 of sCoaT and TM helix 5 of LpCopA) to focus on the structural region that houses residues believed to determine metal-ion specificity.[24] The starting position of TM helices was determined using TMHMM 2.0.[42] In the resultant homology model, residues 227−682 of sCoaT are aligned with residues 291−733 of LpCopA.

Cloning and Expression of Wild-Type sCoaT (WT-sCoaT). The gene sequence encoding the P_{1B-4}-ATPase sCoaT was PCR amplified with PfuTurbo DNA polymerase

(Stratagene) using *Sulfitobacter* sp. NAS-14.1 genomic DNA (ATCC) as a template and the following oligonucleotide primers (Integrated DNA Technologies): forward, 5′-CAC-CGT-GCG-GAA-AGT-CGT-TGC-CGA-T-3′; reverse, 5′-CTA-TGC-CGA-TTT-GAC-GCG-ATT-GTC-CTT-GA-3′. The primers were designed based on PubMed entry GI:83956091 with the introduction of an overhang (underlined) for TOPO cloning. The amplified gene (2.04 kb) was subcloned into the pET151/D-TOPO vector (Invitrogen), which introduces an N-terminal hexahistidine tag with a TEV cleavage site. This vector was transformed into *Escherichia coli* Top10 chemically competent cells (Invitrogen) following the manufacturer's protocol and spread on a Luria-Bertani (LB) agar plate containing 100 μg/mL ampicillin. DNA sequencing (ACGT Inc.) of individual colonies confirmed the gene sequence.

For expression, *E. coli* BL21 Star (DE3) chemically competent cells were transformed with the plasmid encoding sCoaT. Overnight cultures were used to inoculate baffled flasks containing 1 L of LB medium supplemented with 100 mg of ampicillin which were then grown at 37 °C with shaking. Protein expression was induced by the addition of 1 mM IPTG at an OD_{600} of 0.6, at which point the growth temperature was lowered to 18 °C. The cells were harvested after 16−18 h by centrifugation at 4800*g* for 10 min in a Sorvall SLC 4000 rotor at 4 °C, resuspended in 50 mM Tris (pH 7.5), 200 mM NaCl, 500 mM sucrose, and 1 mM PMSF, and stored at −80 °C.

Purification of WT-sCoaT. All purification procedures were carried out at 4 °C. Cells were lysed by sonication for 12 min using 15 s pulses with a 30 s rest period between each pulse. Lysed cells were centrifuged at 8000*g* for 30 min to remove cell debris. The supernatant was then ultracentrifuged at 163000*g* for 1 h. Pelleted membranes were washed once with fresh buffer [50 mM Tris (pH 7.5), 500 mM NaCl, 500 mM sucrose, 1 mM PMSF] and homogenized and then pelleted again by ultracentrifugation at 163000*g* for 45 min. The pelleted, washed membranes were resuspended and homogenized in 25 mM Tris (pH 7.0), 100 mM sucrose, 500 mM NaCl, and 1 mM PMSF and diluted to 3 mg/mL, with the concentration determined by the detergent compatible Lowry assay (Bio-Rad). For solubilization, *n*-dodecyl-β-D-maltopyranoside (DDM) was added dropwise to a final concentration of 1% and allowed to incubate for 1 h at 4 °C with gentle stirring. The suspension was cleared by centrifugation at 163000*g* for 45 min. The supernatant was then applied to a 10 mL Ni^{2+}-loaded HiTrap Chelating HP column (GE Healthcare) and washed with 4 column volumes of 25 mM Tris (pH 7.5), 100 mM NaCl, 20% glycerol, and 0.02% DDM (buffer A), followed by a wash of 6 column volumes of buffer A with 50 mM imidazole. The pure sCoaT protein was eluted with buffer A, containing 300 mM imidazole. Fractions were concentrated in an Amicon 15 mL spin concentrator with a 50 kDa cutoff filter (Millipore), and imidazole was removed by desalting on a HiPrep 26/10 desalting column (GE Healthcare) equilibrated with buffer A. The protein concentration was determined by the Pierce 660 nm protein assay, and protein expression and purification were assessed by 15% SDS−PAGE.

To remove the N-terminal hexahistidine tag, purified sCoaT was treated with TEV protease. A hexahistidyl-tagged TEV protease was added to the purified sCoaT at a 1:2 molar ratio along with 1 mM DTT and incubated at 4 °C with gentle rocking for 16−18 h. The cleavage reaction mixture was then loaded onto a 10 mL Ni^{2+}-loaded HiTrap Chelating HP column (GE Healthcare) and washed with 5 column volumes of buffer A, during which cleaved sCoaT was eluted. Uncleaved sCoaT and hexahistidyl-tagged TEV protease remained bound to the column. Removal of the hexahistidine tag from sCoaT was confirmed by Western blotting, followed by immunostaining with anti-hexahistidine antibody (Sigma Aldrich) and by N-terminal sequence analysis (University of Illinois Champaign-Urbana Protein Sciences Facility).

Cloning, Expression, and Purification of sCoaT Mutants. Mutations S325A, C327A, H657A, E658A, and T661A were introduced using the QuikChange II Site-Directed Mutagenesis kit (Stratagene). Plasmid DNA of pET151/WT-sCoaT was used as template DNA for mutagenesis. The entire sequences of the mutants were verified by automated DNA sequencing (ACGT Inc.). The pET151/mutant plasmids were transformed into *E. coli* BL21 Star (DE3) chemically competent cells, and growth and purification were conducted using the same procedures as those of WT-sCoaT.

ATPase Activity Assay. The metal-dependent ATPase activity of purified sCoaT was measured by the pyruvate kinase−lactate dehydrogenase coupled spectroscopic assay.[17,43] In this assay, regeneration of ATP is coupled to the oxidation of NADH, and enzyme activity is determined by monitoring the decrease of the NADH absorption peak at 340 nm. For activity measurements, sCoaT was exchanged into a buffer containing 25 mM Tris (pH 7.5), 50 mM KCl, 10% glycerol, and 0.02% DDM. The ATPase activity assay mixture (1 mL) contained 50 mM HEPES-KOH (pH 7.5), 100 mM KCl, 0.1% asolectin, 0.1% DDM, 5 mM $MgSO_4$, 0.25 mM NADH, 1.25 mM phosphoenolpyruvate, 9 units of pyruvate kinase, 9 units of lactate dehydrogenase, and 10 μg of sCoaT, with or without Co^{2+}, Pb^{2+}, Zn^{2+}, Cd^{2+}, Cu^{2+}, Cu^{+} (generated from Cu^{2+} in the presence of excess dithiothreitol), and Ni^{2+}. The insolubility of Ag^{+} under the assay conditions precluded testing the Ag^{+}-dependent activity. Assay mixtures were activated by the addition of 5 mM ATP and monitored for 3 min at 25 °C using a Perkin-Elmer LAMBDA 1050 UV−vis spectrophotometer (Keck Biophysics Facility, Northwestern University) at 340 nm.

Metal Loading and Analysis. Purified sCoaT was first exchanged into a buffer containing 25 mM Tris (pH 7.5), 50 mM NaCl, 10% glycerol, and 0.02% DDM using repeated dilution and concentration in an Amicon spin concentrator. Cobalt loading was performed by the addition of 5 molar equiv of $CoCl_2$ to the sCoaT solution, followed by overnight (16−18 h) incubation at 4 °C with gentle rocking. Excess cobalt was removed using an EconoPac 10DG desalting column (Bio-Rad). Metal content was measured by inductively coupled plasma optical emission spectrometry (ICP-OES) using a Varian Vista MPX ICP-OES (Integrated Molecular Structure Education and Research Center, Northwestern University) instrument. All ICP-OES samples were prepared by digestion of the protein in 5 mL of 5% TraceSelect nitric acid (Sigma Aldrich) in Chelexed water, followed by filtration through a 22 μm sterile filter. Cobalt standards for calibration (Sigma Aldrich) were also prepared in 5% nitric acid. Reported ICP-OES results are the average of three replicate experiments performed for at least two independent protein sample preparations. Optical spectra were measured using a Perkin-Elmer LAMBDA 1050 UV−vis instrument.

Electron Paramagnetic Resonance (EPR) Spectroscopy. Samples for EPR spectroscopy were concentrated to 0.6−1 mM Co^{2+} in 25 mM Tris (pH 7.5), 50 mM NaCl, 0.02% DDM, and 50% glycerol. Deuterated samples were prepared in the

same buffer using D_2O and d_8-glycerol (Sigma Aldrich). Samples were transferred to custom Q-band EPR tubes, frozen, and stored in liquid nitrogen. Q-band continuous wave (CW) EPR and electron nuclear double resonance (ENDOR) spectra were collected on a custom-built instrument equipped with a liquid helium immersion dewar at 2 K using 100 kHz field modulation and dispersion mode detection under rapid passage conditions,[44] described previously.[45] Q-band pulsed ENDOR spectra were collected at 2 K on custom-built instruments previously described,[45−47] and the Davies ($\pi-T-\pi/2-\tau-\pi-\tau-$echo) microwave pulse sequence was employed, in which the RF pulse is applied during time period T.[48] All pulse experiment data acquisitions were performed with SpecMan[49] (http://specman4epr.com), in conjunction with a Spin-Core PulseBlaster ESR_PRO 400 MHz word generator and Agilent Technologies Acquiris DP235 500MS/s digitizer.

X-ray Absorption (XAS) Spectroscopy. Samples for XAS were prepared in 25 mM Tris (pH 7.5), 50 mM NaCl, 0.02% DDM, and 50% glycerol with cobalt concentrations in the 1−1.5 mM range. Two independent replicates of cobalt-loaded WT- and C327A-sCoaT were prepared. Samples were loaded into Lucite cells wrapped with Kapton tape, frozen in liquid nitrogen, and stored at −80 °C until data collection. XAS data were collected at the Stanford Synchrotron Radiation Laboratory (SSRL) on beamline 7-3 and at the National Synchrotron Light Source (NSLS) on beamline X3-b. The SSRL beamline was equipped with a Si[220] double crystal monochromator, and the NSLS beamline was equipped with a Si[111] monochromator; both beamlines were equipped with harmonic rejection mirrors. During data collection, samples were maintained at 10 K using an Oxford Instruments continuous-flow liquid helium cryostat at SSRL and at 24 K using a He Displex Cryostat at NSLS. Protein fluorescence excitation spectra were collected using 30-element Ge solid-state detectors at both beamlines. At SSRL, iron filters, 0.3 μm in width, were placed between the cryostat and detector to filter background fluorescence scattering not associated with Co signals. XAS spectra at both facilities were measured in 5 eV increments in the pre-edge regions (7542−7702 eV), 0.25 eV increments in the edge regions (7702−7780 eV), and 0.05 Å^{-1} increments in the extended X-ray absorption fine structure (EXAFS) region (to k = 13.0 Å^{-1}), integrating from 1 to 25 s in a k^3-weighted manner for a total scan length of approximately 40 min. The X-ray energies were individually calibrated by collecting Co foil absorption spectra simultaneously with protein data. The first inflection point of the Co foil spectrum was assigned to 7709.5 eV. Each fluorescence channel of each scan was examined for spectral anomalies prior to averaging, and spectra were closely monitored for photoreduction. SSRL data represent the average of 6 or 7 scans, and NSLS data represent the average of 9 or 10 scans.

XAS data were processed using the Macintosh OS X version of EXAFSPAK[50] integrated with Feff v8[51] for theoretical model generation. Data reduction utilized a Gaussian function in the pre-edge region and a three-region cubic spline throughout the EXAFS region. Data were converted to k space using a cobalt E_0 value of 7725 eV. The k-cubed weighted EXAFS was truncated at 1.0 and 12.5 Å^{-1} for filtering purposes. This k range corresponds to a spectral resolution of ca. 0.14 Å for all cobalt−ligand interactions; therefore, only independent scattering environments outside 0.14 Å were considered resolvable in the EXAFS fitting analysis.[52] EXAFS fitting analysis was performed on raw unfiltered data. EXAFS data were fit using both single- and multiple-scattering amplitudes and phase functions calculated with Feff v8. Single-scattering theoretical models were calculated for carbon, oxygen, sulfur, and cobalt coordination to simulate the copper−nearest neighbor ligand environments. A multiple-scattering Co−imidazole theoretical model was calculated to simulate the numerous scattering interactions observed from the linear ring. A scale factor (Sc) of 0.98% and an E_0 value of −3 eV for a Co−O/N bond, utilized during the protein simulations, were determined by fitting a crystallographically characterized hexaquacobalt(II) nitrate.[53] Criteria for judging the best-fit simulation utilized both the lowest mean-square deviation between data and fit (F′), corrected for the number of degrees of freedom,[54] and a reasonable Debye−Waller factor (σ^2 < 0.006 Å^2).

RESULTS AND DISCUSSION

Homology Modeling. On the basis of sequence alignments, seven conserved residues were proposed to participate in metal binding by P_{1B-4}-ATPases: serine, proline, and cysteine in TM4 and histidine, glutamate, glycine, and threonine in TM6[24] (Figure 2). Additional insight into specific ligands can be obtained by comparison of sCoaT to LpCopA, the only P_{1B}-ATPase structurally characterized to date.[14] Although there are no bound metal ions in the structure, LpCopA is predicted to have two metal-binding sites, one composed of Asn 689, Met 717, and Ser 721 (site I) and the second involving the transmembrane cysteines Cys 382 and Cys 384, as well as Tyr 688 (site II). Homology modeling reveals that four of the putative LpCopA metal-binding residues align with corresponding conserved residues in sCoaT (Figure 2, right). The residues in the SPC motif, Ser 325 and Cys 327, align with LpCopA Cys 382 and Cys 384, respectively, and residues His 657 and Thr 661 align with LpCopA proposed ligands Met 717 and Ser 721, respectively. The other two LpCopA binding residues, Asn 689 and Tyr 688, align with nonconserved valine residues. Conserved sCoaT residue Glu 658 corresponds to an alanine in LpCopA but would be close enough to His 657 and Thr 661 to participate in cobalt binding.

Expression and Purification of WT-sCoaT and Variants. Recombinant expression of WT-sCoaT yielded approximately 2 mg of purified protein/L of cultured medium. Overnight induction of cells at 18 °C increased the yield of purified WT-sCoaT compared to a 3 h induction period at 37 °C. DDM-solubilized WT-sCoaT was purified in a single step by Ni^{2+}-affinity chromatography (Figure 3), and cleavage of the hexahistidine tag using TEV protease yielded ∼70% recovery of untagged WT-sCoaT. The removal of the hexahistidine tag was verified by Western blot using an anti-hexahistidine antibody (Figure 3) and by N-terminal sequence analysis, which indicated complete cleavage. Variant proteins in which Ser 325, Cys 327, His 657, Glu 658, and Thr 661 were mutated to alanine were also prepared to assess the role of these conserved residues in metal binding and activity. These mutants did not express as well as WT-sCoaT, yielding approximately 0.3−0.5 mg of pure protein/L, but utilization of the same WT-sCoaT purification protocol resulted in >90% pure proteins (Figure S1 of the Supporting Information). The low yields precluded TEV protease cleavage of the sCoaT variants, however.

ATPase Activity. The ATPase activity of WT-sCoaT was specifically stimulated by Co^{2+} and was also stimulated by Ni^{2+}, but to a much lesser extent than by Co^{2+} (Figure 4A). None of the other metals tested (Zn^{2+}, Cd^{2+}, Cu^{2+}, Cu^{+}, and Pb^{2+}) were able to activate the enzyme. The Co^{2+}-dependent activity of

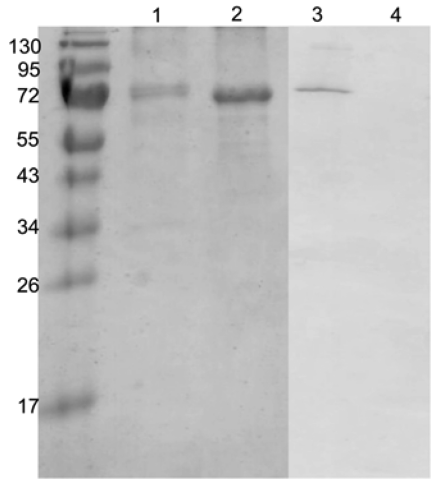

Figure 3. SDS–PAGE and Western analysis of purified WT-sCoaT. Lane 1, SDS–PAGE of purified tagged WT-sCoaT; lane 2, SDS–PAGE of purified TEV-cleaved WT-sCoaT; lane 3, anti-6xHis tag Western blot of purified tagged WT-sCoaT; lane 4, anti-6xHis tag Western blot of purified TEV-cleaved WT-sCoaT.

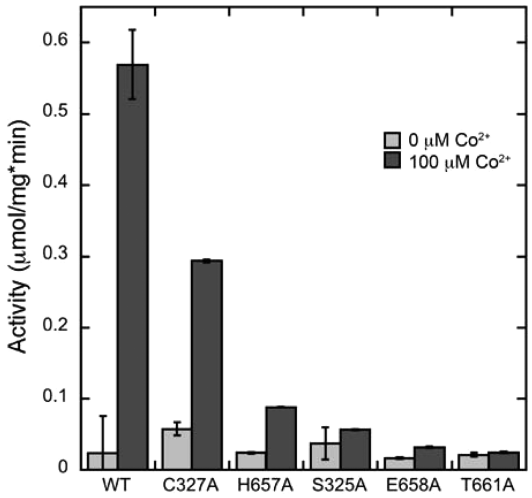

Figure 5. Comparison of ATP hydrolysis activity of WT-sCoaT, C327A-sCoaT, and variants in which His 657, Ser 325, Glu 658, and Thr 661 are replaced with alanine.

WT-sCoaT has a K_M value of 20.05 ± 3.6 μM and a V_{max} value of 0.71 ± 0.03 μmol mg^{-1} min^{-1} (Figure 4B). The V_{max} value is similar to those reported for the Pb^{2+}-stimulated activity of ZntA[17] and the Ag^{+}-stimulated activity of CopA.[19] The activity of the variants was negligible, with the notable exception of the C327A variant (C327A-sCoaT), which has approximately 50% of the WT-sCoaT activity (Figure 5). This result is unexpected and differs from previous studies of P_{1B-1}-, P_{1B-2}-, and P_{1B-3}-ATPases. For *Archaeoglobus fulgidus* CopA, mutation of either cysteine or both cysteines in the CPC motif to alanine abolishes ATPase activity,[26] and in the case of *E. coli* CopA, mutation of these cysteines results in loss of copper resistance, transport, and phosphoenzyme formation.[25] Replacement of either cysteine with alanine in the *E. coli* ZntA CPC motif also results in an inactive enzyme, but ZntA variants in which the cysteines are replaced with histidine retain some activity.[27] For the *Escherichia hirae* CopB Cu^{2+}-ATPase, alteration of the CPH transmembrane motif to SPH abolished the ability to restore copper resistance in a CopB knockout mutant in vivo, suggesting impaired Cu^{2+} transport.[55]

Metal-Binding Stoichiometry. Tagged WT-sCoaT binds 1.55 ± 0.07 Co^{2+} ions per protein monomer, and cleaved WT-sCoaT binds 1.38 ± 0.21 Co^{2+} ions per protein monomer, indicating that the hexahistidyl tag does not bind a significant amount of Co^{2+} during the loading procedure. WT-sCoaT is thus proposed to contain one metal-binding site for Co^{2+}. ZntA from *E. coli* also is reported to contain a single metal-binding site, [35] whereas *A. fulgidus* CopA binds two Cu^{+} ions with high affinity.[56] Interestingly, C327A-sCoaT also appears to have a

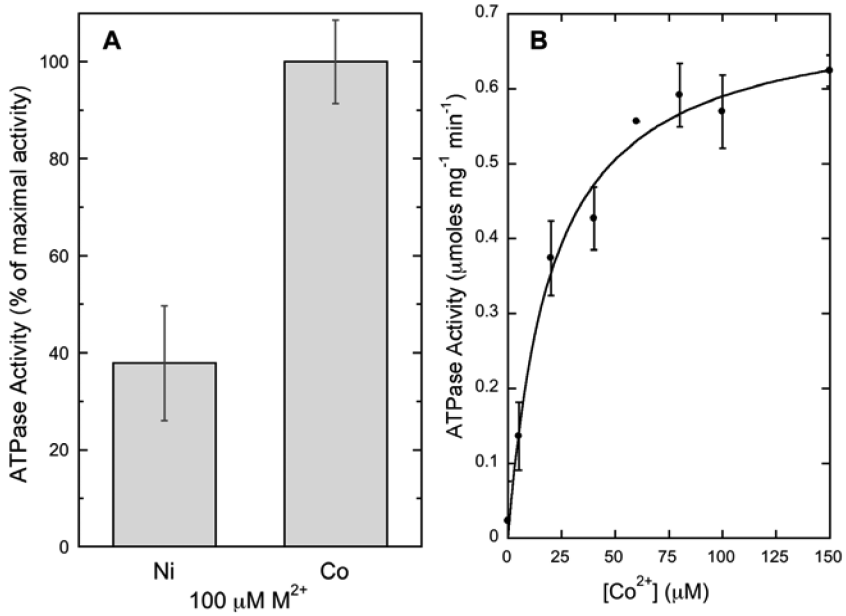

Figure 4. Activity of WT-sCoaT. (A) Co^{2+} stimulates the highest ATP hydrolysis activity. Results are the average of at least three independent replicates. Maximal activity for 100 μM Co^{2+} is 0.57 μmol of ATP mg^{-1} min^{-1}. (B) Co^{2+} stimulates ATPase activity of WT-sCoaT. Fits were performed using Kaleidagraph software with the equation $y = (V_{max}x)/(K_M + x)$.

dx.doi.org/10.1021/bi3006708 | *Biochemistry* 2012, 51, 7891–7900

single Co^{2+}-binding site, with a stoichiometry of 1.49 ± 0.53 Co^{2+} ions per monomer. This result suggests that the cysteine in the TM metal-binding SPC motif is not essential for Co^{2+} binding and is consistent with the observation of ATPase activity for C327A-sCoaT (Figure 5). None of the other mutants were able to bind Co^{2+}, a further indication that the hexahistidyl tag does not bind Co^{2+}. This finding is consistent with the lack of ATPase activity of these variants and indicates that Ser 325, His 657, Glu 658, and Thr 661 are essential for Co^{2+} binding and activity and may be ligands as predicted by the homology modeling based on the LpCopA structure.

The optical spectra of Co^{2+}-loaded WT-sCoaT and C327A-sCoaT both exhibit a broad shoulder extending from the 280 nm protein absorbance to ~400 nm (Figure 6). Although this

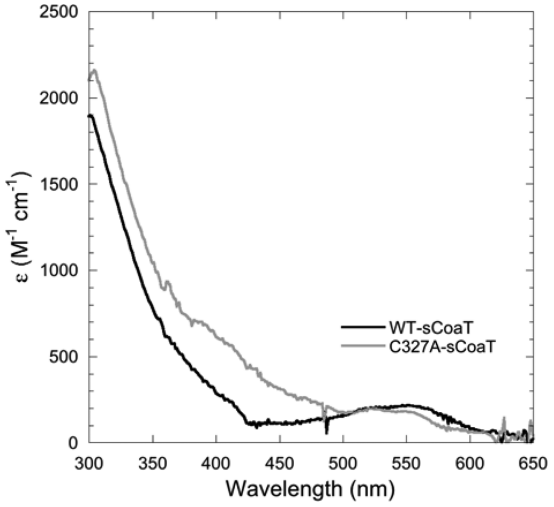

Figure 6. Difference spectra of the Co^{2+}-bound forms of WT- and C327A-sCoaT, using the respective apo forms as reference spectra.

region of the spectrum is typically associated with Co^{2+}-thiolate ligand-to-metal charge transfer (LMCT) bands, the lack of distinct peaks observed for these intense transitions[57−59] and the similarity between the spectra of WT-sCoaT and the cysteine-lacking C327A-sCoaT suggest that this absorbance does not arise from interactions with sulfur ligands. This shoulder is more likely attributable to histidine-to-Co^{2+} LMCT and resembles features observed in the spectrum of Co^{2+}-substituted copper, zinc superoxide dismutase.[60] The geometry of Co^{2+} sites can be correlated with the position and intensity of d−d transitions in the visible region.[59,61] The broad features in the 500−600 nm region of the sCoaT spectra ($\varepsilon \sim 300\ M^{-1}\ cm^{-1}$) are most consistent with regular tetrahedral geometry.[61,62] The shift of the peak in C237A-sCoaT toward ~525 nm may indicate some distortion of the Co^{2+}-binding site, perhaps due to perturbation of the secondary coordination environment.

EPR and ENDOR. WT-, tagged WT-, and C327A-sCoaT all exhibit an $S = 3/2$ Co^{2+} EPR signal with a broad feature at $g_\perp$ = 3.9 and $g_\parallel \sim 2$, consistent with tetrahedral symmetry.[63] Tagged and untagged WT-sCoaT show identical EPR signals, indicating that Co^{2+} does not bind to the hexahistidyl tag (Figure 7A). The presence of the same feature in the C327A-sCoaT spectrum indicates that the Co^{2+} coordination sphere is not altered by deletion of the conserved cysteine residue.

ENDOR spectra collected at $g_\perp$ = 3.9 from WT-, C327A-, and tagged WT-sCoaT (Figure 7B), reveal identical signals

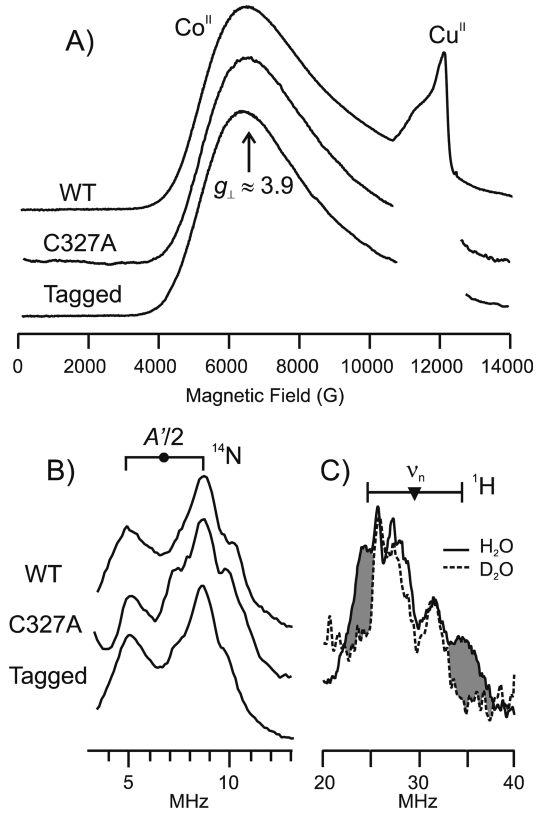

Figure 7. 35 GHz EPR and ENDOR spectra. (A) Absorption-display CW Q-band EPR spectra of tagged WT-sCoaT, C327A-sCoaT, and WT-sCoaT at 2 K. Each sample exhibits an $S = 3/2$ Co^{2+} signal as characterized from the broad feature at $g_\perp = 3.9$. Adventitious Cu^{2+} in variable amounts is observed at higher fields, but no copper can be detected in the samples by ICP-OES. (B) ^{14}N Davies ENDOR spectra taken near $g_\perp$. Goalpost centered at $A'/2$, split by $2 \times \nu_n(^{14}N)$. (C) ^1H CW ENDOR spectra of WT-CoaT in ^1H_2O (solid line) and ^2H_2O buffer (dashed line) taken near $g_\perp$. Shading highlights the intensity from an exchangeable proton. Goalpost centered at $\nu(^1H)$, split by A'. CW EPR and ENDOR conditions include microwave frequency, 34.9 GHz; modulation amplitude, 2 G; time constant, 32 ms; EPR scan time, 4 min; ENDOR scan rate, 2 MHz/s. Pulse ENDOR conditions include microwave frequency, 34.6 GHz; π, 80 ns; τ, 600 ns; T_{RF}, 30 μs; repetition rate, 20 ms.

from a single, strongly coupled ^{14}N. The signal is a doublet of broad peaks that is centered at half the hyperfine coupling of A' = 13.6 MHz,[45] with a separation of twice the ^{14}N nuclear Larmor frequency. This coupling treats the Co^{2+} as having an effective spin, $S' = 1/2$; in an $S = 3/2$ representation the hyperfine coupling is A = 21.0 MHz, comparable to the histidine bound to Cu^{2+}, $S = 1/2$. The observed hyperfine coupling A', taken at a given g value, is modified from the intrinsic A value. $A' = gA/g_e$. The higher-frequency (ν_+) partner shows a poorly resolved structure that indicates the Co^{2+} site is structurally heterogeneous, with several contributing conformers; an additional contribution from the nuclear quadrupole interaction in at least one conformer may also be present. An attempt to measure this interaction with ESEEM spectroscopy failed because rapid spin dephasing quenched the spin−echo modulation. The strongly coupled nitrogen can be assigned to a bound histidine residue, based on the near identity of its signal to that of a histidine bound to Co^{2+} of the Zn-finger in the transcription factor IIIA (TFIIIA) from *Xenopus laevis*.[64] This residue is very likely to be His 657,

dx.doi.org/10.1021/bi3006708 | *Biochemistry* 2012, 51, 7891−7900

which is found in transmembrane helix 6 of sCoaT (Figure 2), is conserved in the P_{1B-4} subgroup, and has been proposed to be a metal-binding ligand.[24] The equivalence of the ^{14}N signals from untagged and tagged WT-sCoaT shows that there is no coordination to Co^{2+} by a residue from the hexahistidine tag. The equivalence of the ^{14}N signals from WT-sCoaT and C327A-sCoaT, like the invariance of the EPR signal, indicates that the C327A mutation does not alter the Co^{2+} coordination sphere. Lastly, ^{1}H ENDOR spectra taken near $g_{\perp}$ exhibit a ^{1}H doublet, hyperfine coupling $A' = 13$ MHz, that is lost when the sample is prepared with $^{2}H_2O$ buffer. As this coupling is of the magnitude expected from the proton(s) of an H_xO coordinated along the $g_{\|}$ direction, these observations indicate that Co^{2+} binds a single aqua species.

XAS Spectroscopy. The XANES spectra of WT- and C327A-sCoaT resemble that of $Co(NO_3)_2{\cdot}6H_2O$ (Figure 8),

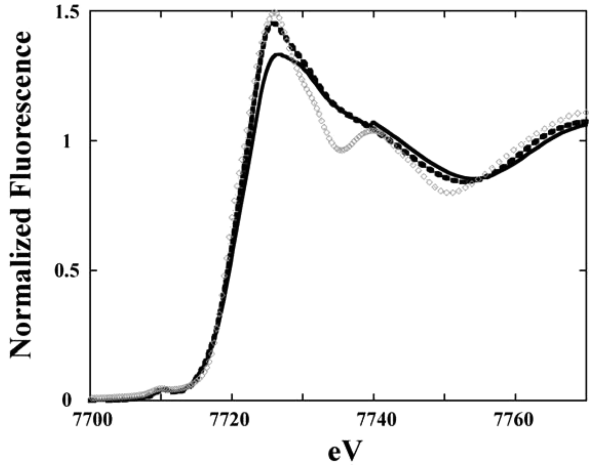

Figure 8. Normalized XANES spectra of Co-bound WT- (solid) and C327A-sCoaT (dashed line) displayed with the spectrum of solid $Co(NO_3)_2$ (gray triangles).

indicating that cobalt is stable in the divalent redox state and most likely dominated by the coordination of oxygen/nitrogen-based ligands. The Fourier transforms of the EXAFS spectrum for Co^{2+} bound to WT- and C327A-sCoaT suggest complex patterns of the Co−nearest neighbor ligand environments at $R < 3$ Å, with additional scattering patterns of ligands at $R > 3$ Å (Figure 9). Best-fit simulations of the WT- and C327A-sCoaT Co EXAFS indicate a nearest neighbor environment constructed completely of oxygen- and/or nitrogen-based ligands. Nearest neighbor metrical parameters include a short Co−O/N distance at 1.95 and 1.96 Å, and a longer distance set of Co−O/N ligands at 2.14 and 2.12 Å for WT- and C327A-sCoaT, respectively. The shorter ∼1.95 Å distances are highly reminiscent of the values observed for four-coordinate Co−O small molecule compounds in the Cambridge structural database, whereas the longer ∼2.13 Å distance would be consistent with Co−imidazole nitrogen distances.[65] Long-range carbon scattering environments at ca. 3.1, 3.5, and 4.1 Å are also consistent with imidazole multiple-scattering interactions expected for histidines coordinated to Co[66] (Table 1). There is no evidence for a Cu−S interaction in the EXAFS, consistent with the activity assays, metal-binding studies, UV−vis, and EPR data, indicating that Cys 327 of the SPC motif is not involved in Co^{2+} binding. Moreover, the presence of only oxygen/nitrogen ligands is compatible with the predicted

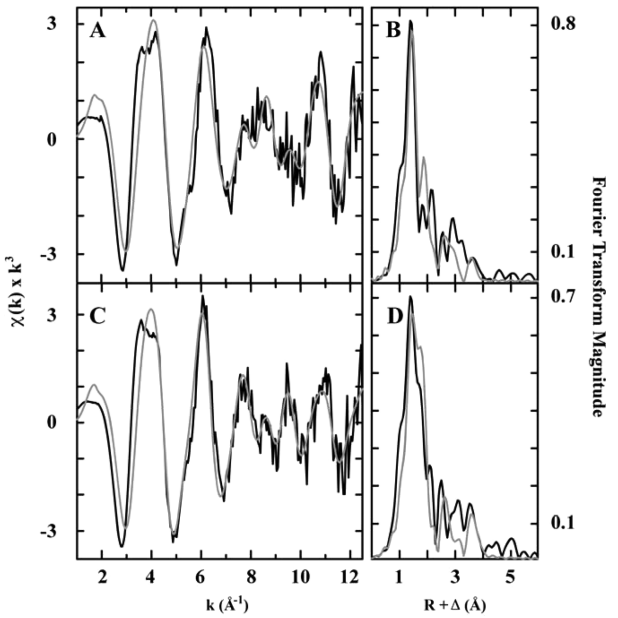

Figure 9. EXAFS and Fourier transform for WT- and C327A-sCoaT. Raw unfiltered EXAFS data (black) and simulations (gray) for cobalt bound to (A) WT- and (C) C327A-sCoaT. Fourier transforms of the raw EXAFS (black) and best-fit simulations (gray) for cobalt bound to (B) WT- and (D) C327A-sCoaT.

metal-binding residues that are conserved in the P_{1B-4} subclass, including the serine in TM4, and the histidine, glutamate, and threonine residues in TM6 (Figure 2). The observed imidazole multiple-scattering interactions support the EPR data and are consistent with His 657 in TM4 being a ligand.

Implications for the sCoaT Metal-Binding Site. The combined data on the WT-sCoaT and sCoaT variants indicate the presence of a single Co^{2+}-binding site that is coordinated by nitrogen and oxygen ligands, including a histidine and a water molecule, in a tetrahedral geometry. Surprisingly, the data indicate that the cysteine residue in the conserved SPC transmembrane metal-binding motif is not directly involved in Co^{2+} binding in this state of the enzyme. In several P_{1B}-ATPases that contain cysteines in this motif (vide supra), such as *E. coli* CopA, *A. fulgidus* CopA, *E. hirae* CopB, and *E. coli* ZntA, the transmembrane cysteines appear to play essential and equivalent roles in the catalytic cycle.[25−27,55] However, in other P_{1B}-ATPases, the cysteine residues in this motif are believed to be nonequivalent and function at different stages of the transport mechanism. For example, mutation of both cysteines in *Saccharomyces cerevisiae* Ccc2 yields no in vivo or ATPase activity, but phosphorylation by ATP is still possible for a CPC to SPC variant, although not for a CPC to CPS variant. These findings indicate that the second cysteine is necessary for metal binding at the transport site, whereas the first cysteine plays a role in metal dissociation and/or enzyme dephosphorylation.[67] Similarly, mutation of either cysteine in the CPC motif of CadA, a $Zn^{2+}/Cd^{2+}/Pb^{2+}$-ATPase from *Listeria monocytogenes*, inhibits in vivo Cd^{2+} transport, but only the CPC to CPA variant retains the ATP hydrolysis activity. In addition, the CPA variant can be phosphorylated by ATP, suggesting that the first cysteine is more directly involved in Cd^{2+} binding, and the second cysteine may participate in occlusion and release.[29] The data for C327A-sCoaT are consistent with this type of scenario in which Cys 327 does not play a role in initial Co^{2+} binding and catalytic steps involving the E1 conformation (Figure 1)

dx.doi.org/10.1021/bi3006708 | *Biochemistry* 2012, 51, 7891−7900

Table 1. Summary of Best-Fit EXAFS Simulations for Cobalt Bound to WT- and C327A-sCoaT[a]

	nearest neighbor ligand environment[b]				long range ligand environment[c]				
sample	atom[d]	R (Å)[e]	CN[f]	σ^{2}[g]	atom[d]	R (Å)[e]	CN[f]	σ^{2}[g]	F'[h]
WT	O/N	1.95	2	3.62	C	3.04	1	5.21	0.49
	O/N	2.14	2	3.42	C	3.33	1	3.62	
					C	4.09	1	3.31	
C327A	O/N	1.96	1	1.97	C	3.03	1	4.85	0.49
	O/N	2.12	3	5.69	C	3.39	0.5	3.15	
					C	4.08	2	5.06	

[a]Data fit over a k range of 1−12.5 Å^{-1}. [b]Independent metal−ligand scattering environment at R < 3.0 Å. [c]Independent metal−ligand scattering environment at R > 3.0 Å. [d]Scattering atoms: O (oxygen), N (nitrogen), C (carbon). [e]Average metal−ligand bond length for multiple independent samples. [f]Average metal−ligand coordination number for multiple independent samples. [g]Average Debye−Waller factor in Å^2 × 10^3 for multiple independent samples. [h]Number of degrees of freedom weighted mean-square deviation between data and fit.

but may play a role in the E2 conformation, perhaps participating in metal release or dephosphorylation. Taken together, our data indicate that Co^{2+} can bind in the absence of the TM4 cysteine and that histidine, probably His 657, and water are coordinated. Besides His 657, Ser 325, Glu 658, and Thr 661 are also necessary for Co^{2+} binding and transport and thus likely comprise the additional nitrogen and oxygen ligands. Further studies to elucidate the molecular details of Co^{2+} coordination are underway.

■ ASSOCIATED CONTENT

Supporting Information

SDS−PAGE analysis of purified sCoaT mutants. This material is available free of charge via the Internet at http://pubs.acs.org.

■ AUTHOR INFORMATION

Corresponding Author

*A.C.R.: e-mail, amyr@northwestern.edu; tel, 847-467-5301; fax, 847-467-6489. T.L.S.: e-mail, tstemmle@med.wayne.edu; tel, 313-577-5712; fax, 313-577-2765.

Funding

This work was supported by NIH Grants GM58518 (A.C.R.), DK068139 (T.L.S.), and HL13531 (B.M.H.). E.L.Z. was supported in part by NIH Grant 5T32 GM008382. G.E.C. was supported by NSF Fellowship DGE-0824162.

Notes

The authors declare no competing financial interest.

■ ACKNOWLEDGMENTS

Portions of this research were carried out at both the Stanford Synchrotron Radiation Laboratory (SSRL) and the National Synchrotron Light Source (NSLS). SSRL is a national user facility operated by Stanford University on behalf of the U.S. Department of Energy, Office of Basic Energy Sciences. The SSRL Structural Molecular Biology Program is supported by the Department of Energy, Office of Biological and Environmental Research, and by the NIH, National Center for Research Resources, Biomedical Technology Program. NSLS, located at Brookhaven National Laboratory, is supported by the U.S. Department of Energy, Division of Materials Sciences and Division of Chemical Sciences, under Contract DE-AC02-98CH10886.

■ ABBREVIATIONS

sCoaT, *Sulfitobacter* sp. NAS-14.1 P_{1B-4}-ATPase; WT-sCoaT, wild-type sCoaT; C327A-sCoaT, variant sCoaT in which Cys 327 is replaced with alanine; LpCopA, L. pneumophila Cu^+ P_{1B-1}-ATPase; ATPBD, ATP binding domain; N-domain, nucleotide binding domain; P-domain, phosphorylation domain; A-domain, actuator domain; SDS−PAGE, sodium dodecyl sulfate−polyacrylamide gel electrophoresis.

■ REFERENCES

(1) Bublitz, M., Morth, J. P., and Nissen, P. (2011) P-type ATPases at a glance. *J. Cell Sci. 124*, 2515−2519.

(2) Palmgren, M. G., and Nissen, P. (2011) P-Type ATPases. *Annu. Rev. Biophys. 40*, 243−266.

(3) Axelsen, K. B., and Palmgren, M. G. (1998) Evolution of substrate specificities in the P-type ATPase superfamily. *J. Mol. Evol. 46*, 84−101.

(4) Bublitz, M., Poulsen, H., Morth, J. P., and Nissen, P. (2010) In and out of the cation pumps: P-Type ATPase structure revisited. *Curr. Opin. Struct. Biol. 20*, 431−439.

(5) Lutsenko, S., and Kaplan, J. H. (1995) Organization of P-type ATPases: Significance of structural diversity. *Biochemistry 34*, 15607−15613.

(6) Albers, R. W. (1967) Biochemical aspects of active transport. *Annu. Rev. Biochem. 36*, 727−756.

(7) Post, R. L., Hegyvary, C., and Kume, S. (1972) Activation by adenosine triphosphate in the phosphorylation kinetics of sodium and potassium ion transport adenosine triphosphatase. *J. Biol. Chem. 247*, 6530−6540.

(8) Solioz, M., and Camakaris, J. (1997) Acylphosphate formation by the Menkes copper ATPase. *FEBS Lett. 412*, 165−168.

(9) Voskoboinik, I., Mar, J., Strausak, D., and Camakaris, J. (2001) The regulation of catalytic activity of the Menkes copper-translocating P-type ATPase. *J. Biol. Chem. 276*, 28620−28627.

(10) Møller, J. V., Olesen, C., Winther, A. M. L., and Nissen, P. (2010) The sarcoplasmic Ca^{2+}-ATPase: Design of a perfect chemi-osmotic pump. *Q. Rev. Biophys. 43*, 501−566.

(11) Morth, J. P., Pedersen, B. P., Toustrup-Jensen, M. S., Sorensen, T. L. M., Petersen, J., Andersen, J. P., Vilsen, B., and Nissen, P. (2007) Crystal structure of the sodium-potassium pump. *Nature 450*, 1043−1049.

(12) Shinoda, T., Ogawa, H., Cornelius, F., and Toyoshima, C. (2009) Crystal structure of the sodium-potassium pump at 2.4 angstrom resolution. *Nature 459*, 446−450.

(13) Pedersen, B. P., Buch-Pedersen, M. J., Morth, J. P., Palmgren, M. G., and Nissen, P. (2007) Crystal structure of the plasma membrane proton pump. *Nature 450*, 1111−1114.

(14) Gourdon, P., Liu, X. Y., Skjørringe, T., Morth, J. P., Møller, L. B., Pedersen, B. P., and Nissen, P. (2011) Crystal structure of a copper-transporting PIB-type ATPase. *Nature 475*, 59−74.

(15) Rensing, C., Mitra, B., and Rosen, B. P. (1997) The *zntA* gene of *Escherichia coli* encodes a Zn(II)-translocating P-type ATPase. *Proc. Natl. Acad. Sci. U.S.A. 94*, 14326−14331.

(16) Rensing, C., Sun, Y., Mitra, B., and Rosen, B. P. (1998) Pb(II)-translocating P-type ATPases. *J. Biol. Chem. 273*, 32614−32617.

(17) Sharma, R., Rensing, C., Rosen, B. P., and Mitra, B. (2000) The ATP hydrolytic activity of purified ZntA, a Pb(II)/Cd(II)/Zn(II)-translocating ATPase from *Escherichia coli*. *J. Biol. Chem. 275*, 3873–3878.
(18) Mana-Capelli, S., Mandal, A. K., and Argüello, J. M. (2003) *Archaeoglobus fulgidus* CopB is a thermophilic Cu^{2+}-ATPase. *J. Biol. Chem. 278*, 40534–40541.
(19) Mandal, A. K., Cheung, W. D., and Argüello, J. M. (2002) Characterization of a thermophilic P-type Ag^{+}/Cu^{+}-ATPase from the extremophile *Archaeglobus fulgidus*. *J. Biol. Chem. 277*, 7201–7208.
(20) Raimunda, D., González-Guerrero, M., Leeber, B. W., and Argüello, J. M. (2011) The transport mechanism of bacterial Cu^{+}-ATPases: Distinct efflux rates adapted to different function. *BioMetals 24*, 467–475.
(21) Rutherford, J. C., Cavet, J. S., and Robinson, N. J. (1999) Cobalt-dependent transcriptional switching by a dual-effector MerR-like protein regulates a cobalt-exporting variant CPx-type ATPase. *J. Biol. Chem. 274*, 25827–25832.
(22) Lutsenko, S., Gupta, A., Burkhead, J. L., and Zuzel, V. (2008) Cellular multitasking: The dual role of human Cu-ATPases in cofactor delivery and intracellular copper balance. *Arch. Biochem. Biophys. 476*, 22–32.
(23) Bull, P. C., and Cox, D. W. (1994) Wilson disease and Menkes disease: New handles on heavy-metal transport. *Trends Genet. 10*, 246–252.
(24) Argüello, J. M. (2003) Identification of ion-selectivity determinants in heavy-metal transport P_{1B}-type ATPases. *Membr. Biochem. 195*, 93–108.
(25) Fan, B., and Rosen, B. P. (2002) Biochemical characterization of CopA, the *Escherichia coli* Cu(I)-translocating P-type ATPase. *J. Biol. Chem. 277*, 46987–46992.
(26) Mandal, A. K., and Argüello, J. M. (2003) Functional roles of metal binding domains of the *Archaeoglobus fulgidus* Cu^{+}-ATPase CopA. *Biochemistry 42*, 11040–11047.
(27) Dutta, S. J., Liu, J. B., Stemmler, A. J., and Mitra, B. (2007) Conservative and nonconservative mutations of the transmembrane CPC motif in ZntA: Effect on metal selectivity and activity. *Biochemistry 46*, 3692–3703.
(28) Okkeri, J., and Haltia, T. (2006) The metal-binding sites of the zinc-transporting P-type ATPase of *Escherichia coli*. Lys(693) and Asp(714) in the seventh and eighth transmembrane segments of ZntA contribute to the coupling of metal binding and ATPase activity. *Biochim. Biophys. Acta 1757*, 1485–1495.
(29) Wu, C. C., Gardarin, A., Martel, A., Mintz, E., Guillain, F., and Catty, P. (2006) The cadmium transport sites of CadA, the Cd^{2+}-ATPase from *Listeria monocytogenes*. *J. Biol. Chem. 281*, 29533–29541.
(30) Argüello, J. M., Eren, E., and González-Guerrero, M. (2007) The structure and function of heavy metal transport P_{1B}-type ATPases. *BioMetals 20*, 233–248.
(31) González-Guerrero, M., Hong, D., and Argüello, J. M. (2009) Chaperone-mediated Cu^{+} delivery to Cu^{+} transport ATPases. Requirement of nucleotide binding. *J. Biol. Chem. 284*, 20804–20811.
(32) Hatori, Y., Majima, E., Tsuda, T., and Toyoshima, C. (2007) Domain organization and movements in heavy metal ion pumps: Papain digestion of CopA, a Cu^{+}-transporting ATPase. *J. Biol. Chem. 282*, 25213–25221.
(33) Eren, E., Kennedy, D. C., Maroney, M. J., and Argüello, J. M. (2006) A novel regulatory metal binding domain is present in the C terminus of *Arabidopsis* Zn^{2+}-ATPase HMA2. *J. Biol. Chem. 281*, 33881–33891.
(34) Barry, A. N., Shinde, U., and Lutsenko, S. (2010) Structural organization of human Cu-transporting ATPases: Learning from building blocks. *J. Biol. Inorg. Chem. 15*, 47–59.
(35) Liu, J. B., Dutta, S. J., Stemmler, A. J., and Mitra, B. (2006) Metal-binding affinity of the transmembrane site in ZntA: Implications for metal selectivity. *Biochemistry 45*, 763–772.
(36) Okkeri, J., and Haltia, T. (1999) Expression and mutagenesis of ZntA, a zinc-transporting P-type ATPase from *Escherichia coli*. *Biochemistry 38*, 14109–14116.
(37) Traverso, M. E., Subramanian, P., Davydov, R., Hoffman, B. M., Stemmler, T. L., and Rosenzweig, A. C. (2010) Identification of a hemerythrin-like domain in a P_{1B}-type transport ATPase. *Biochemistry 49*, 7060–7068.
(38) Scherer, J., and Nies, D. H. (2009) CzcP is a novel efflux system contributing to transition metal resistance in *Cupriavidus metallidurans* CH34. *Mol. Microbiol. 73*, 601–621.
(39) Moreno, I., Norambuena, L., Maturana, D., Toro, M., Vergara, C., Orellana, A., Zurita-Silva, A., and Ordenes, V. R. (2008) AtHMA1 is a thapsigargin-sensitive Ca^{2+} heavy metal pump. *J. Biol. Chem. 283*, 9633–9641.
(40) Seigneurin-Berny, D., Gravot, A., Auroy, P., Mazard, C., Kraut, A., Finazzi, G., Grunwald, D., Rappaport, F., Vavasseur, A., Joyard, J., Richaud, P., and Rolland, N. (2006) HMA1, a new Cu-ATPase of the chloroplast envelope, is essential for growth under adverse light conditions. *J. Biol. Chem. 281*, 2882–2892.
(41) Guex, N., and Peitsch, M. C. (1997) SWISS-MODEL and the Swiss-PdbViewer: An environment for comparative protein modeling. *Electrophoresis 18*, 2714–2723.
(42) Krogh, A., Larsson, B., von Heijne, G., and Sonnhammer, E. L. L. (2001) Predicting transmembrane protein topology with a hidden Markov model: Application to complete genomes. *J. Mol. Biol. 305*, 567–580.
(43) Vogel, G., and Steinhart, R. (1976) ATPase of *Escherichia coli*: Purification, dissociation, and reconstitution of the active complex from the isolated subunits. *Biochemistry 15*, 208–216.
(44) Mailer, C., and Hoffman, B. M. (1976) Tumbling of an adsorbed nitroxide using rapid adiabatic passage. *J. Phys. Chem. 80*, 842–846.
(45) Werst, M. M., Davoust, C. E., and Hoffman, B. M. (1991) Ligand spin densities in blue copper proteins by Q-band ^{1}H and ^{14}N ENDOR spectroscopy. *J. Am. Chem. Soc. 113*, 1533–1538.
(46) Davoust, C. E., Doan, P. E., and Hoffman, B. M. (1996) Q-band pulsed electron spin-echo spectrometer and its application to ENDOR and ESEEM. *J. Magn. Reson. 119*, 38–44.
(47) Zipse, H., Artin, E., Wnuk, S., Lohman, G. J. S., Martino, D., Griffin, R. G., Kacprzak, S., Kaupp, M., Hoffman, B., Bennati, M., Stubbe, J., and Lees, N. (2009) Structure of the nucleotide radical formed during reaction of CDP/TTP with the E441Q-$\alpha 2\beta 2$ of *E. coli* ribonucleotide reductase. *J. Am. Chem. Soc. 131*, 200–211.
(48) Schweiger, A., and Jeschke, G. (2001) *Principles of Pulse Electron Paramagnetic Resonance*, Oxford University Press, Oxford, U.K.
(49) Epel, B., Gromov, I., Stoll, S., Schweiger, A., and Goldfarb, D. (2005) Spectrometer Manager: A Versatile Control Software for Pulse EPR Spectrometers. *Concepts Magn. Reson., Part B 26B*, 36–45.
(50) George, G. N., George, S. J., and Pickering, I. J. (2001) *EXAFSPAK*. http://www-ssrl.slac.stanford.edu/~george/exafspak/exafs.htm.
(51) Ankudinov, A. L., and Rehr, J. J. (1997) Relativistic calculations of spin-dependent X-ray absorption spectra. *Phys. Rev. B: Condens. Matter Mater. Phys. 56*, R1712–R1715.
(52) Lee, P. A., Citrin, P. H., Eisenberger, P., and Kincaid, B. M. (1981) Extended X-ray absorption fine structure: Its strengths and limitations as a structural tool. *Rev. Mod. Phys. 53*, 769–806.
(53) Prelesnik, B. V., Gabela, F., Ribar, B., and Krstanovic, I. R. (1973) Hexaquacobalt(II) nitrate, $Co[OH_2]_6[NO_3]_2$. *Cryst. Struct. Commun. 2*, 581–583.
(54) Bencze, K. Z., Kondapalli, K. C., and Stemmler, T. L. (2007) X-ray absorption spectroscopy. In *Applications of Physical Methods to Inorganic and Bioinorganic Chemistry: Handbook, Encyclopedia of Inorganic Chemistry* (Scott, R. A., and Lukehart, C. M., Eds.) 2nd ed., pp 513–528, John Wiley & Sons, Ltd., Chichester, U.K.
(55) Bissig, K.-D., Wunderli-Ye, H., Duda, P. W., and Solioz, M. (2001) Structure-function analysis of purified *Enterococcus hirae* CopB copper ATPase: Effect of Menkes/Wilson disease mutation homologues. *Biochem. J. 357*, 217–223.
(56) González-Guerrero, M., Eren, E., Rawat, S., Stemmler, T. L., and Argüello, J. M. (2008) Structure of the two transmembrane Cu^{+} transport sites of the Cu^{+}-ATPases. *J. Biol. Chem. 283*, 29753–29759.

(57) Regan, L., and Clarke, N. D. (1990) A tetrahedral zinc(II)-binding site introduced into a designed protein. *Biochemistry 29*, 10878−10883.
(58) May, S. W., and Kuo, J. Y. (1978) Preparation and properties of cobalt(II) rubredoxin. *Biochemistry 17*, 3333−3338.
(59) Bertini, I., and Luchinat, C. (1984) High spin cobalt(II) as a probe for the investigation of metalloproteins. *Adv. Inorg. Biochem. 6*, 71−111.
(60) Salvato, B., Beltramini, M., Ricchelli, F., and Tallandini, L. (1989) Cobalt substitution studies on bovine erythrocyte superoxide dismutase: Evidence for a novel cobalt-superoxide dismutase derivative. *Biochim. Biophys. Acta 998*, 14−20.
(61) Lever, A. B. P. (1984) *Inorganic Electronic Spectroscopy*, 2nd ed., Elsevier Science Publishing Company, Inc., New York.
(62) Brader, M. L., Kaarsholm, N. C., Harnung, S. E., and Dunn, M. F. (1997) Ligand perturbation effects on a pseudotetrahedral Co(II)$(His)_3$-ligand site. *J. Biol. Chem. 272*, 1088−1094.
(63) Makinen, M. W., Kuo, L. C., Yim, M. B., Wells, G. B., Fukuyama, J. M., and Kim, J. E. (1985) Ground term splitting of high-spin Co^{2+} as a probe of coordination structure. 1. Dependence of the splitting on coordination geometry. *J. Am. Chem. Soc. 107*, 5245−5255.
(64) Walsby, C. J., Krepkiy, D., Petering, D. H., and Hoffman, B. M. (2003) Cobalt-substituted zinc finger 3 of transcription factor IIIA: Interactions with cognate DNA detected by P-31 ENDOR spectroscopy. *J. Am. Chem. Soc. 125*, 7502−7503.
(65) Allen, F. H. (2002) The Cambridge Structural Database: A quarter of a million crystal structures and rising. *Acta Crystallogr. B58*, 380−388.
(66) Feiters, M. C., Navaratnam, S., Alhakim, M., Allen, J. C., Spek, A. L., Veldink, G. A., and Vliegenthart, J. F. G. (1988) EXAFS of poly[μ-hexakis(2-methylimidazolato-*N*,*N*′)triiron(II)]: Implications for metalloprotein studies. *J. Am. Chem. Soc. 110*, 7746−7750.
(67) Lowe, J., Vieyra, A., Catty, P., Guillain, F., Mintz, E., and Cuille, M. (2004) A mutational study in the transmembrane domain of Ccc2p, the yeast Cu(I)-ATPase, shows different roles for each Cys-Pro-Cys cysteine. *J. Biol. Chem. 279*, 25986−25994.